Photovoltaic-based Distributed Generation Allocation in Distribution Network for Energy Loss Minimization

Mansur Khasanov[1][*], *Salah* Kamel[2], *Francisco* Jurado[3], *Abror* Kurbanov[4] and *Urinboy* Jalilov[4]

[1]Tashkent State Technical University, 100095 Tashkent, Uzbekistan
[2]Department of Electrical Engineering, Faculty of Engineering, Aswan University, 81542 Aswan, Egypt
[3]Department of Electrical Engineering, University of Jaen, 23700 EPS Linares, Jaen, Spain
[4]Department of Energy, Faculty of Energy and radio electronics, Jizzakh Polytechnic Institute, Jizzakh, Uzbekistan

Abstract. Nowadays, there is a global consensus that integrating renewable energy sources (RESs) is highly needed to meet the increasing electricity demand and reduce the overall carbon footprint of energy production. However, large-scale integration of RES-based distributed generation (DG) units often poses several technical challenges in the system from stability, reliability, and power quality perspectives. However, these problems are usually mitigated by the optimal integration of DG units in the distribution networks (DNs). In this regard, the optimal sizing and placement of the DGs are crucial. Otherwise, network performance will deteriorate. This paper proposes to apply a novel population-based technique called the dung beetle optimization (DBO) algorithm for the optimal allocation of Photovoltaic (PV) based DG units to minimize total active energy loss subject to equality and inequality constraints in the DN. A DBO is inspired by the behaviours of dung beetles, including ball-rolling, dancing, foraging, stealing, and reproducing. A standard 33-bus system has been used to demonstrate the proposed method's effectiveness. The simulation results and comparison with other techniques demonstrate our proposed approach's significant energy loss reduction and a suitable voltage profile.

1. Introduction

As a result of a variety of technical, economic, and structural factors, the adoption of renewable energy sources (RESs) is booming worldwide. In other words, RES integration in DNs is growing globally. Energy consumption is rising globally, inefficient energy production methods are causing pollution, and climate change is a concern. These factors contribute to RESs' significant integration into the energy system. [1-2]. RES integration goals are being set by policymakers in numerous nations worldwide [3]. According to the article in [4], it is predicted that as a result of the integration of RES into the mainstream energy generation system, traditional energy production from oil, gas, and coal - which are currently supplying about 80% of total energy demand worldwide - will gradually decrease over time. RES developments—primarily wind turbine (WT), photovoltaic (PV), and geothermal—are on the rise, although their contribution to primary energy is still relatively small, at 0.5%. Changing from conventional to "clean" energy generation paradigms involves a variety of social, environmental, economic, political, and technological challenges [5]. With these adjustments, developing standards for environmental and renewable policies is necessary to develop a new value chain. Geopolitical shifts in the energy sector will result from the development of such initiatives [6]. Many electrical DNs have seen a steady rise in RES-based DG units.

However, there are some difficulties with RES integration [7]. The nature of such resources is the biggest challenge. As a result of the natural volatility of these resources and their partial unpredictability (uncertainty), it isn't very easy to operate, control, and plan for the power system. Further, integrating RES-based DG units at a large scale often presents several technical challenges regarding system reliability, stability, and power quality. However, the optimal

---

[*]Corresponding author: hasanov6654525@mail.ru

integration of DG units in DNs usually mitigates these problems. It is crucial to size and position the DGs optimally in this regard. Otherwise, the network's performance will deteriorate if an allocation is not done correctly.

Until now, a considerable amount of research has been devoted to determining the most effective allocation and sizing of RES-based DG units in DNs, particularly concerning hybrid planning. There has been a recent shift towards utilizing optimization methods based on metaheuristics, such as the Harris Hawks Optimizer (HHO) [8], and Hybrid approach (HA) [9], An efficient analytical (EA) and Particle swarm optimization (PSO) [10], the Hybrid salp swarm algorithm (HSSA) [11]. The Electrostatic discharge algorithm (ESDA) was employed in [12] to minimize power losses and enhance voltage stability by allocating DG units. Furthermore, Mansur et al. proposed an Artificial ecosystem-based optimization approach that reduces annual power losses through optimal sizing and location of DG units in the DNs [13].

In this paper, an accurate algorithm called DBO proposed for optimizing the placement and size of PV-based DG units in DN is presented to reduce the total energy loss of the DN. Loss-Sensitivity Factor (LSF) is employed to speed up the solution process and determine suitable candidate buses. Furthermore, solar irradiation variability is characterized using the Beta Probability Distribution Function (PDF). A standard 33-bus system has been used to demonstrate the proposed method's effectiveness and compared to other techniques published in the literature to address the same problem it addresses.

The structure of the paper is as follows: Section 2 provides a detailed description of LSF. A probabilistic power generation model for PV-based DGs and a load model are presented in Section 3. The problem formulation is presented in Section 4. The solution process of the proposed technique is presented in Section 5. Section 6 describes numerical results, and Section 7 concludes the paper with conclusions.

2. Loss Sensitivity Factor (LSF)

LSF is used in this paper to determine the candidate buses for reducing the search space. An equivalent grid-connected two-bus DN is shown in Figure 1, used to illustrate this factor.
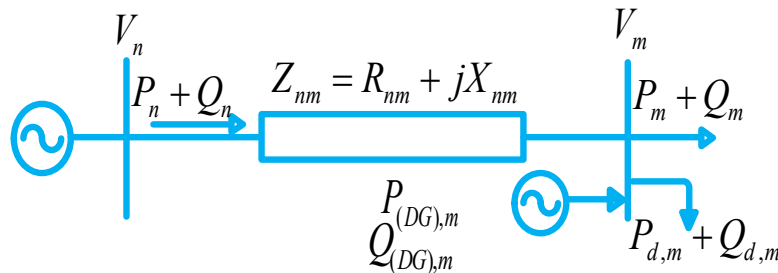
Fig. 1. The radial DN with two buses that are connected to the grid and DG unit is represented in the equivalent diagram

where, P_n and P_m are two active power flows emanating from the bus n and m, Q_n and Q_m are two reactive power flows emanating from the bus n and m, V_n and V_m are represents the voltage magnitude of buses n and m. R_{nm} and X_{nm} are the resistance and reactance of the distribution line between buses n and m, respectively. At bus m $P_{DG,m}$ is the active power output of PV-based DG, while $Q_{DG,m}$ is the reactive power output, $P_{d,m}$ and $Q_{d,m}$ are representing the active and reactive power loads at same bus.

The following formula is used to calculate power loss:

$$P_{nm-loss} = \frac{(P_m^2 + Q_m^2) * R_{nm}}{(V_m)^2} \tag{1}$$

To calculate the LSF, we use equation (3)

$$\frac{\partial P_{nm-loss}}{\partial Q_m} = \frac{2Q_m * R_{nm}}{(V_m)^2} \tag{2}$$

Figure 2 shows the LSFs for the 33-bus test system. LSFs are sorted in descending order after calculating them for all buses. A bus with a higher LSF is considered more suitable for PV installation (up to 50% of system buses) [14,15].
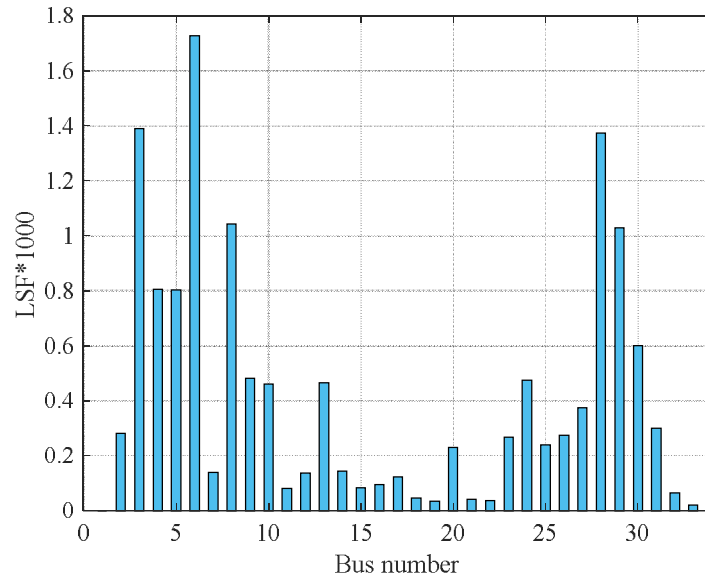
Fig. 2. A 33-bus test system's LSF values

3. The probabilistic power generation of PV-based DG and load modelling

3.1. A PV model for generating power

Temperature and solar radiation play an essential role in determining PV power generation. To get reasonable solutions, it is necessary to accurately model solar radiation at a certain location. By analyzing collected historical data for hourly solar radiation per day, we determine the standard deviation (SD) and mean. The continuous probability distribution function (PDF) of each PV-based DG unit is divided into states (periods), in each of which the solar irradiance lies within specified limits so that the output power of each PV-based DG unit can be taken into consideration as multistate variables in the planning formulation. Alternatively, the solar irradiance comprises several states for each time segment [15]. A solar radiation state of 0.05 kW/m^2 is used in this paper. In this state, the output power is calculated based on the average value of each state (e.g., if the first state of solar radiation falls between 0 and 0.05 kW/m^2, the average value for this state is 0.025 kW/m^2).

3.1.1 Modeling of solar radiation: The Beta PDF [16] describes the probabilistic nature of solar radiation. Beta PDF is defined as (3) for time interval t for solar radiation S (kW/m2).

$$f_{beta}(S^t) = \begin{cases} \dfrac{G(\alpha^t + \beta^t)}{G(\alpha^t)G(\beta^t)} S^{t(\alpha^t-1)}(1-S^t)^{(\beta^t-1)}, & 0 \leq S^t \leq 1, \quad \alpha^t, \beta^t \geq 0 \\ 0, & otherwise \end{cases} \tag{3}$$

where, $f_{beta}(S^t)$ is the Beta PDF of S^t, α^t and β^t represent the Beta PDF's shape rates, and G represents gamma's function.

The Beta PDF's shape rates for a suitable time interval can be found using mean (μ) and SD (σ) of solar radiation:

$$\beta^t = (1-\mu^t)\left(\frac{\mu^t(1+\mu^t)}{\sigma^{t2}} - 1\right) \tag{4.1}$$

$$\alpha^t = \frac{\mu^t * \beta^t}{1-\mu^t} \tag{4.2}$$

3.1.1.1 Power generation from PV arrays: An estimated PV array hourly power output corresponds to a time interval 't' (P^t_{PV}), expressed as (5). Figure 4 illustrates the average power generated for a day of 3 years in p.u.

$$P^t_{PV} = \sum_{m=1}^{N_s} P_{PV_o}(s^t_m) f_{beta}(s^t_m) \tag{5}$$

where 'm' is the state factor, and N_s is the total solar radiation state number in the study period. S^t_m is represents solar radiation at t^{th} time interval and the mth state.

A PV array's power output is primarily influenced by solar radiation and ambient temperature. Based on the average solar radiation (S_{avm}) for the mth state, it is estimated that PV power will be generated as follows:

$$P_{PV_o}(s_{avm}) = N_{PV\,mod} * FF * V_m * I_m \tag{6}$$

where, N_{PVmod} is the total number of PV modules in the system. The following equations can determine the PV module the voltage-ampere characteristic for a given state [14]:

$$FF = \frac{V_{MPP} * I_{MPP}}{V_{OC} * I_{SC}} \tag{7.1}$$

$$V_m = V_{OC} - K_v * T_{cm} \tag{7.2}$$

$$I_m = s_{avm}\left[I_{SC} + K_i(T_C - 25)\right] \tag{7.3}$$

$$T_{cm} = T_A + s_{avm}\left(\frac{N_{OT} - 20}{0.8}\right) \tag{7.4}$$

here, $T_A(°C)$ represents ambient temperature, V_{MPP} is the maximum power tracking voltage, and I_{MPP} is the maximum power tracking current, V_{OC} and I_{SC} represent open-circuit and short circuit voltage and currents of PV module, K_i and K_v are temperature coefficients (A/°C and V/°C), FF is fill factor of PV module, T_{cm} represents at m^{th} state temperature (°C) of PV module.

3.2. Load modeling

As shown in Figure 3, the proposed load model uses a 24-hour daily load curve with a peak of 1 p.u. [17]. To calculate the load factor (LF), the following equation can be used:
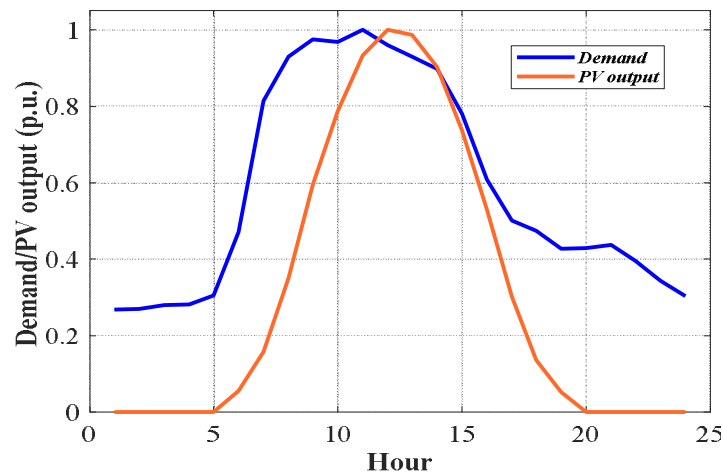
Fig. 3. Normalized PV output power and active load curves

$$LF = \sum_{t=1}^{24} \frac{p.u.\,Demand(t)}{24} \tag{8}$$

Load demand varies with time and voltage in a voltage-dependent model. In consequence, it can be calculated that the voltage-dependent load demand model in [17], which includes variable loads at the time t, can be expressed as follows:

$$P_m(t) = P_{om}(t) * V_m^{n_p}$$
$$Q_m(t) = Q_{om}(t) * V_m^{n_q} \tag{9}$$

where P_m and Q_m represents active and reactive power of bus m; P_{om} and Q_{om} are similarly base active and reactive load at bus m; V_m is the voltage at bus m, and n_P=1.51 and n_q=3.4 are voltage indexes [17].

4. Problem formulation

Minimizing total energy losses in a DN can be achieved by integrating the PV-based DG units at the optimal locations and sizes, considering the operational constraints.

The energy loss (E_{loss}) during 24 hours can be expressed in the following formula:

$$E_{loss} = \sum_{t=1}^{24} P_{nm-loss}(t)\Delta t \tag{10}$$

where, Δt is the time step, in this paper (1 h).

4.1 Equality restrictions:
For the total generated power, the following constraints must be met:

$$P_{sub} + \sum_{l=1}^{M_{DG}} P_{DG}(l) = \sum_{l=1}^{L} P_{Lineloss}(l) + \sum_{l=1}^{M} P_d(l) \tag{11.1.}$$

$$Q_{sub} + \sum_{l=1}^{M_{DG}} Q_{DG}(l) = \sum_{l=1}^{L} Q_{Lineloss}(l) + \sum_{l=1}^{M} Q_d(l) \tag{11.2.}$$

where, P_{sub} and Q_{sub} are the substation's active and reactive power. M_{DG} is the total DG number, M is the total line number in the system.

4.2 Inequality restrictions:
Voltage restrictions:
There are specific voltage requirements between the lower and upper limits of the bus voltage. The requirements are as follows:

$$V_{min} \le |V_i| \le V_{max} \tag{12}$$

The power constraint of integrated DG units is as follows [9]:

$$P_{DG}^{min} \le P_{DG}(i) \le P_{DG}^{max} \tag{13.1}$$

$$Q_{DG}^{min} \le Q_{DG}(i) \le Q_{DG}^{max} \tag{13.2.}$$

Here, the maximum and minimum active power of DG units are indicated as P_{DG}^{min} and P_{DG}^{max}. Similarly, the reactive power of DG units are indicated as Q_{DG}^{min} and Q_{DG}^{max}, respectively.

The power factor limits of DG are as follows:

$$PF_{DG,min} \le PF_{DG,i} \le PF_{DG,max} \tag{14}$$

where, $PF_{DG,min}$ and $PF_{DG,max}$ are lower and upper limits of PF.

Branch capacity limitation:
The maximum capacity of the branch must meet the following limits:

$$S_{Li} \le S_{Li(rated)} \tag{15}$$

5. Overview of the dung beetle optimization (DBO) algorithm

An optimization algorithm inspired by the ball-rolling, dancing, foraging, stealing, and reproduction behaviours of dung beetles is known as the dung beetle optimization (DBO) algorithm [18]. The dung beetle is well known as one of the most common insects in nature, and it feeds off the waste products that animals produce. It should be noted that dung beetles are common in most parts of the planet and act as decomposers in the natural world, which demonstrates their importance in maintaining a healthy ecosystem by decomposing dead organisms.

This algorithm consists of the following steps:

1.   At first, Initialization of the positions of dung beetles randomly.

$$x_i = x_{min} + (x_{max} - x_{min}) * rand \tag{16}$$

where, x_{min} and x_{max} are the lower and upper limits of the optimization dimension.

2.   Calculate the fitness function values of all dung beetles and determine the global best position and its fitness value by descending all the objective values.

$$fit(x_i) \tag{17}$$

3.   Update the locations of all dung beetles. To do this, generate a r1 random number within (0,1).
       If r1 is smaller than 0.9, update locations as follows:

$$x_i(t+1) = x_i(t) + \alpha * k * x_i(t-1) + b * \Delta x \tag{18}$$

where, Δx is used to simulate light intensity changes.

$$\Delta x = |x_i(t) - X_{worst}| \tag{19}$$

t is the current iteration number, $x_i(t)$ is the position of ith dung beetle at the tth iteration, k is deflection coefficient k ∈ (0, 0.2], b is a constant value between (0,1), α is the natural coefficient can be -1 or 1, X_{worst} is global worst position of dung beetles.
       If r1 is large than 0.9, update locations as follows:

$$x_i(t+1) = x_i(t) + \tan(\theta)|x_i(t) - x_i(t-1)| \tag{20}$$

where, θ is the deflection angle belonging to [0, π].

4.   Calculate the fitness function values of all updated dung beetle's positions and determine the current best position and its fitness value by descending all the objective values.

$$fit(x_i) \tag{21}$$

5.   Do boundary selection strategy by using the following equation:

$$x_{min}^* = \max(X^* * (1-w), x_{min})$$
$$x_{max}^* = \min(X^* * (1+w), x_{max}) \tag{22}$$

where, x_{min}^* and x_{max}^* are lower and upper bounds of the spawning area, respectively. X^* represents the current local best position. w is step size by lapse of iterations and calculated as follows:

$$w = 1 - \frac{t}{T_{max}} \tag{23}$$

T_{max} is the sated maximum iteration number.

6.   As soon as the spawning area is identified, the female dung beetles lay their eggs on the brood balls. Note that in this algorithm, female dung beetles are 20 % of all dung beetles number.
The position of the brood ball is updated as follows:

$$B_i(t+1) = X^* + b_1 * (B_i(t) - x_{min}^*) + b_2 * (B_i(t) - x_{max}^*) \tag{24}$$

where, $B_i(t)$ is the position of the *i*th brood ball at the *t*th iteration, b_1 and b_2 are independent random vectors and its size 1× optimization dimension.

7.   Calculate the fitness function values of the brood ball position and determine the current best position and its fitness value by descending all the objective values.

$$fit(B_i) \tag{25}$$

8.   Update position of the small dung beetle can be expressed as (26). Note that in this algorithm, small dung beetles are 20 % of all dung beetles number.

$$X_i(t+1) = X_i(t) + C_1 * (X_i(t) - x_{min}^{**}) + C_2 * (x_i(t) - x_{max}^{**}) \tag{26}$$

where, C_1 is a random number produced by normal PDF, and C_2 is a random vector belonging to (0, 1). x_{min}^{**} and x_{max}^{**} are lower and upper limits of the optimal foraging area, respectively and calculated as follows:

$$x_{min}^{**} = \max(X^{**} * (1-w), x_{min})$$
$$x_{max}^{**} = \min(X^{**} * (1+w), x_{max}) \tag{26}$$

X^{**} is the global best position

9.   Calculate the fitness function values of the small dung beetles position and determine the current best position and its fitness value by descending all the objective values.

$$fit(X_i) \tag{27}$$

10.   A type of dung beetle known as a thief is believed to steal dung balls from other dung beetles to protect their nest. Note that thieves' dung beetles are 30 % of all dung beetles' numbers in this algorithm. The thief is updated their position and can be expressed as follows:

$$X^{thief}_i(t+1) = X^{**} + S*g*\left(\left|X^{thief}_i(t) - X^*\right| + C_2*\left|X^{thief}_i(t) - X^{**}\right|\right) \tag{28}$$

where, $X^{thief}_i(t)$ is position of the ith thief at the tth iteration. g is random vector and its size $1\times$ optimization dimension. S is constant value and its equal to 0.5 in this algorithm.

11.   Calculate the fitness function values of thief dung beetles position and determine current best position and its fitness value by descending all the objective values.

$$fit(X^{thief}_i) \tag{29}$$

12.   Update the individual's best fitness value and the global best fitness value.
13.   To get the global optimal solution and its fitness value, repeat the steps above until t meets the termination criterion.

Table 1 represents the parameters and operational limits of the proposed technique for solving objective function.

Table 1. Used parameters and operational constraints

Parameters	Values
Number of search agents	30
Number of iterations	100
Bus system voltage constraints	$0.9\,p.u. \leq V_i \leq 1.05\,p.u.$
DG power generation limits	$0.2MW \leq P_{DG,m} \leq 3MW$

6. Results and Discussion

This section uses a standard 33-bus test system to evaluate the proposed approach. The simulation has been carried out using MATLAB R2021b software. The following scenarios are considered to demonstrate the effectiveness of the proposed approach:

First scenario: This scenario aims to determine the most efficient PV-based DG unit allocation at unity power factor to minimize power losses without considering voltage-dependent time-varying loads.

Second scenario: the uncertainty power generation model is utilized with time-varying commercial load demands to minimize energy loss.

An illustration of a single-line diagram of a test system can be found in Figure 4. The system has a base kV and MVA of 12.66 kV and 100 MVA for 33 bus DN. There are 3715 kW of active and 2300 kVAr of reactive power loads in the 33-bus test system. There is an initial active power loss of 210.9824 kW and a minimum voltage of 0.904 p.u. for the test system. In [19] provides additional information for the test system.
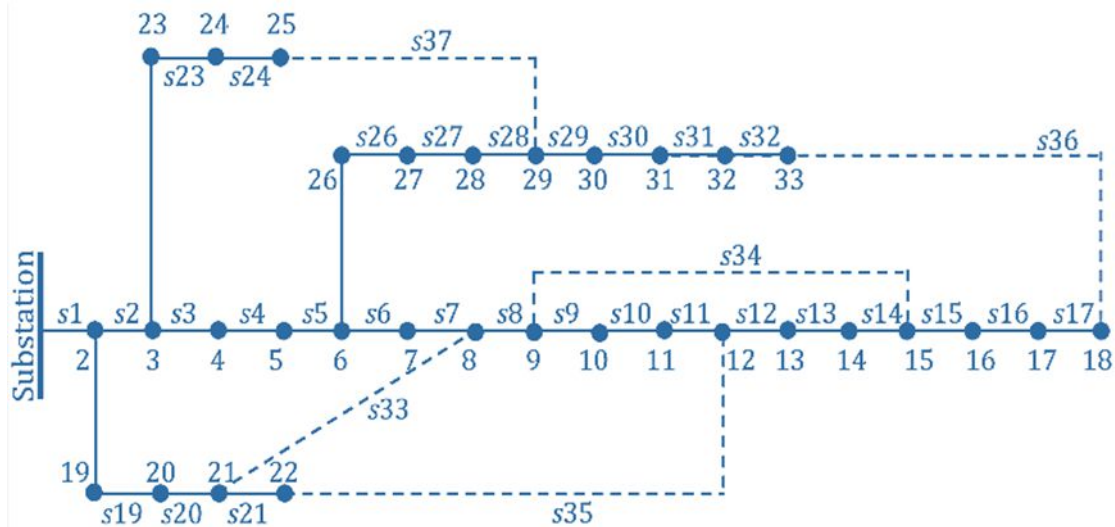
Fig. 4. The line diagram of the test system

Scenario 1: Table 2 summarizes the results of the proposed method for scenario 1 for determining the optimal size and location of PV-based DG units in the 33-bus system to minimize power loss. It can be seen from the table that for integrating one, two and three PV-based DG units in DN, the percentages of active power loss reduction were 47.3761%, 58.6854% and 65.5013%. Based on the analysis of Table 2, it appears that the proposed algorithm is capable of providing the least amount of power loss when it comes to PV-based DG units both in case of one and multiple units' integration, in comparison to EA, HA, HSSA, PSO, and HHO.

Table 2. Comparison of GMO simulation results of the 33-bus system

Type and number of DG		HHO [8]	HA [9]	EA [10]	HSSA [11]	PSO [10]	**GMO**
One PV	Bus (Size (KW /P.F))	6(2590.2/1)	6(2530/1)	6(2530/1)	6(2590.2/1)	6(2590/1)	**6(2590.21/1)**
	Power loss (KW)	111.035	111.42	111.07	111.027	111.03	**111.0271**
Two PV	Bus (Sizes (KW /P.F))	30(1150.6/1) 13(855.93/1)	13(844/1) 30(1149/1)	13(844/1) 30(1149/1)	30(1157.6/1) 13(851.5/1)	13(850/1) 30(1160/1)	**13(851.5/1) 30(1157.6/1)**
	Power loss (KW)	87.1682	87.43	87.172	87.166	87.170	**87.165**
Three PV	Bus (Sizes (KW /P.F))	14 (790.3/1) 24 (870/1) 30(1119.51/1)	13 (798/1) 30(1050/1) 24(1099/1)	13(798/1) 30(1050) 24 (1099)	30(1053.6/1) 24(1091.3/1) 13(801.7/1)	14(770/1) 30(1070/1) 24(1090/1)	**13(801.71/1) 30(1053.6/1) 24(1091.3/1)**
	Power loss (KW)	73.4478	72.79	72.79	72.786	72.790	**72.786**

Scenario 2: In Scenario 2, the power generation uncertainty model of PV is addressed by using the optimal locations and sizes that have been determined in Scenario 1, as well as the time-varying daily commercial load demand, which can be seen in Figure 3.

Table 3. Daily energy losses of the test system

Scenarios	Energy Losses (kW h)	Reduction %
Base case	2044.8	-
With three PV-based DG units	1036.1	49
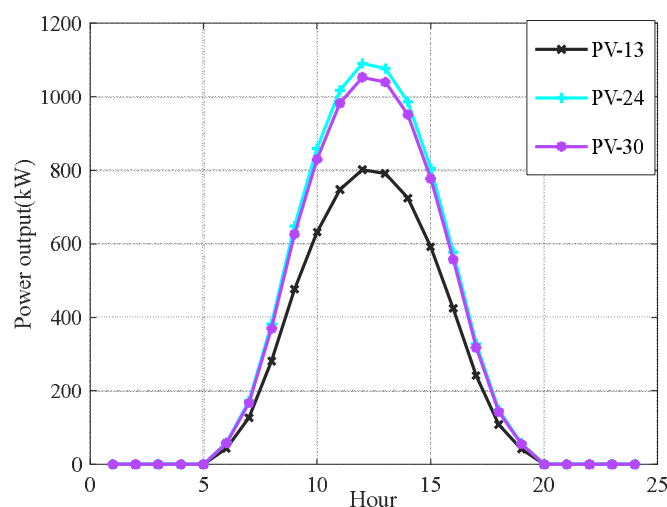
Fig. 5. Daily 3 PV-based DG units power generation curve for the test system
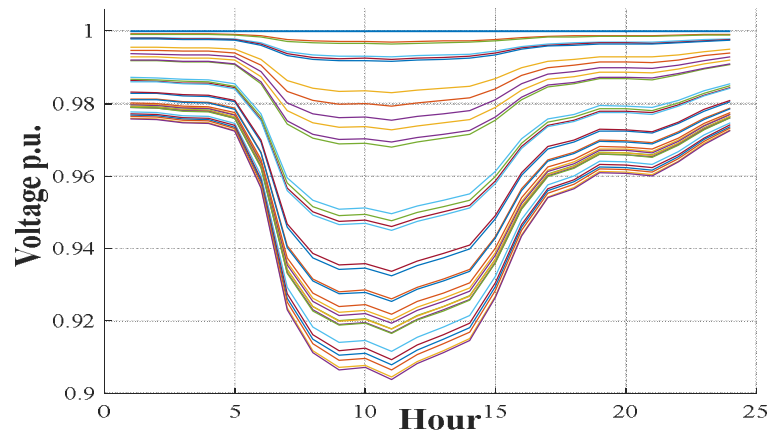
Fig. 6. The voltage profile of the test system (base case)
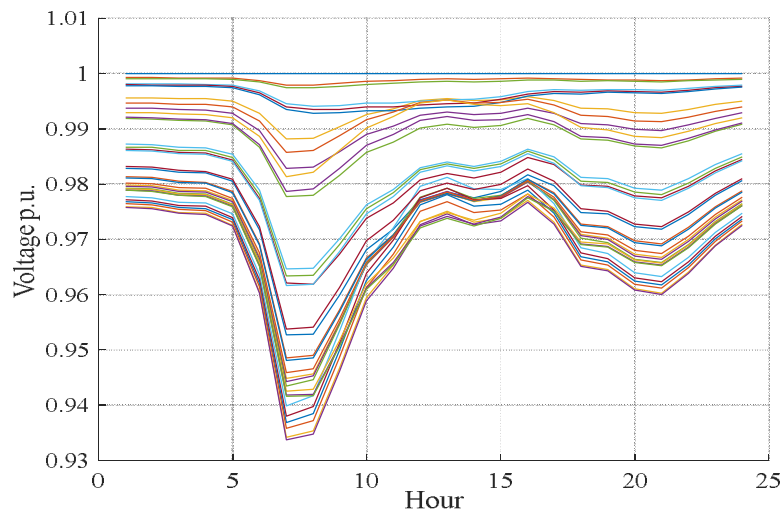
Fig. 7. The voltage profile of the test system (with integrated three PV-based DG units)
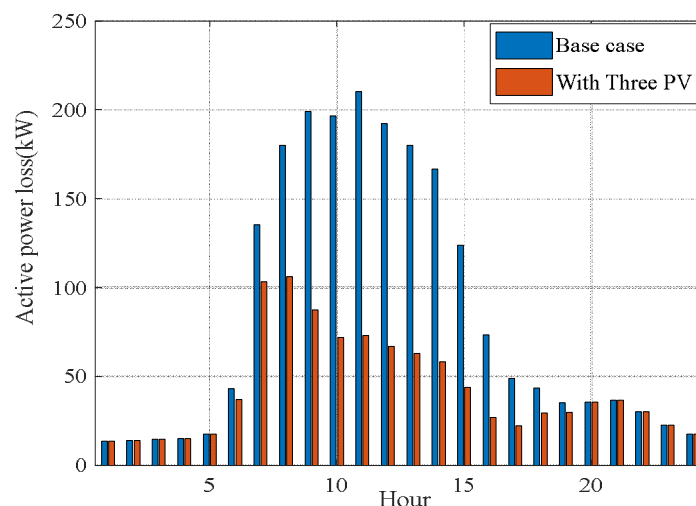
Fig. 8. Three PV-based DG units' integration effect on active energy losses

It is shown in Figure 5 that three PV units have been installed in buses 24, 13 and 30 and are capable of generating power 24 hours a day. It is shown in Figures 6-7 that the effect of load variability on the voltage profile of the standard 33-bus over the course of 24 hours can be seen. It is shown in Figure 8 that a 33-bus DN is conducted in a

9

base case and the potential impact of the installation of PV on energy losses. As compared to base case, there is a noticeable decrease in energy loss. Integrating PV-based DG units leads to a decline in the highest energy loss. Table 3 presents the total energy loss and the reduction of that loss on a particular day.

7. Conclusions

In this paper, a new metaheuristic DBO algorithm combined with the LSI method has been proposed and employed to calculate optimal allocations of single and multiple PV-based DG units, taking into account the voltage-dependent time-varying load demand, along with the probabilistic of PV power generation. The Beta PDF model has been used to describe the stochastic nature of solar radiation. The objective function has been considered to be minimizing the active energy loss of DNs. A standard 33-bus system has been used to demonstrate the proposed method's effectiveness. Three PV-based DG units were considered to test the feasibility of the combined method on the energy loss minimization and have a closer look at the impact of PV DG units on voltage profile. A comparison has been made between the proposed method's performance and the performance of other algorithms used for the same problem in the literature. Furthermore, the results indicate that integrating three PV units into the 33-bus system can reduce energy losses by 49 % compared to the base case.

References

1. J. Yan, et al., Clean, efficient and affordable energy for a sustainable future, *Applied Energy* **185**, 953-962 (2017)
2. R. Adib, et al., Renewables 2015 global status report, *REN21 Secretariat, Paris, France* 162 (2015)
3. A. Aslani, H. Petri, N. Marja, Role of renewable energy policies in energy dependency in Finland: System dynamics approach, *Applied energy* **113**, 758-765 (2014)
4. Y. Wang, Zh. Sheng, H. Huo, Cost and CO2 reductions of solar photovoltaic power generation in China: Perspectives for 2020, *Renewable and Sustainable Energy Reviews* **39**, 370-380 (2014)
5. A. Colmenar-Santos et al., Distributed generation: A review of factors that can contribute most to achieve a scenario of DG units embedded in the new distribution networks, *Renewable and Sustainable Energy Reviews* **59**, 1130-1148 (2016)
6. B. Fais et al., Comparing different support schemes for renewable electricity in the scope of an energy systems analysis, *Applied energy* **131**, 479-489 (2014)
7. P.S. Georgilakis, D.H. Nikos, Optimal distributed generation placement in power distribution networks: models, methods, and future research, *IEEE Transactions on power systems* **28.3**, 3420-3428 (2013)
8. M. Khasanov et al., Optimal distributed generation and battery energy storage units integration in distribution systems considering power generation uncertainty, *IET Generation, Transmission & Distribution* **15.24**, 3400-3422 (2021)
9. S. Kansal, K. Vishal, T. Barjeev, Hybrid approach for optimal placement of multiple DGs of multiple types in distribution networks, *International Journal of Electrical Power & Energy Systems* **75**, 226-235 (2016)
10. K. Mahmoud, Y. Naoto, A. Abdella, Optimal distributed generation allocation in distribution systems for loss minimization, *IEEE Transactions on power systems* **31.2**, 960-969 (2015)
11. H. Abdel-Mawgoud et al., Hybrid Salp Swarm Algorithm for integrating renewable distributed energy resources in distribution systems considering annual load growth, *Journal of King Saud University-Computer and Information Sciences* **34.1**, 1381-1393 (2022)
12. M. Khasanov, K. Salah, H. Abdel-Mawgoud, Minimizing power loss and improving voltage stability in distribution system through optimal allocation of distributed generation using electrostatic discharge algorithm, *2019 21st International Middle East Power Systems Conference (MEPCON)*. IEEE (2019)
13. M. Khasanov et al., Allocation of photovoltaic and wind turbine-based DG units using artificial ecosystem-based optimization, *2020 IEEE International Conference on Environment and Electrical Engineering and 2020 IEEE Industrial and Commercial Power Systems Europe (EEEIC/I&CPS Europe)*, IEEE (2020)
14. M. Khasanov et al., Optimal distributed generation and battery energy storage units integration in distribution systems considering power generation uncertainty, *IET Generation, Transmission & Distribution* **15.24**, 3400-3422 (2021)
15. M. Khasanov et al., Optimal allocation strategy of photovoltaic-and wind turbine-based distributed generation units in radial distribution networks considering uncertainty, *Neural Computing and Applications* **35.3**, 2883-2908 (2023)
16. D.Q. Hung, M. Nadarajah, R.C. Bansal, Integration of PV and BES units in commercial distribution systems considering energy loss and voltage stability, *Applied energy* **113**, 1162-1170 (2014)

17. D.Q. Hung, M. Nadarajah, K.Y. Lee, Optimal placement of dispatchable and nondispatchable renewable DG units in distribution networks for minimizing energy loss, *International Journal of Electrical Power & Energy Systems* **55**, 179-186 (2014)
18. J. Xue, Sh. Bo, Dung beetle optimizer: A new meta-heuristic algorithm for global optimization, *The Journal of Supercomputing* **79.7**, 7305-7336 (2023)
19. M.E. Baran, F.F. Wu, Network reconfiguration in distribution systems for loss reduction and load balancing, *IEEE Transactions on Power Delivery* **4** (2), 1401–1407 (1989)